Predicting Transmittance Spectra of Electrophotographic Color Prints

Safer Mourad[1], Patrick Emmel[2] and Roger David Hersch[2]

[1]Eidgenössische Materialprüfungs- und Forschungsanstalt (EMPA)
[2]Ecole Polytechnique Fédérale de Lausanne (EPFL)

ABSTRACT

For dry toner electrophotographic color printers, we present a numerical simulation model describing the color printer response based on a physical characterization of the different electrophotographic process steps. The proposed model introduces a *Cross Transfer Efficiency* designed to predict the color transmittance spectra of multi-color prints by taking into account the transfer influence of each deposited color toner layer upon the other layers.

The simulation model leads to a better understanding of the factors that have an impact on printing quality. In order to avoid the additional optical non-linearities produced by light reflection on paper (dot-gain), we have limited the present investigation to transparency prints. The proposed model succeeded to predict the transmittance spectra of printed wedges combining two color toner layers with a mean deviation less than CIE-LAB $\Delta E = 2.5$.

Keywords: Electrophotographic printing, electrophotographic process model, color prediction, device calibration

1. INTRODUCTION

Observed under a microscope, the dots of electrophotographic prints appear mostly like clouds of randomly distributed toner particles. Occasionally, the particles are deposited beyond their target area and form extremely ragged dot edges. This high dot distortion causes the major difficulty in estimating the color of electrophotographically printed patches and affects the tone reproduction curve. Virtually all classical color prediction models are still based on a regular dot shape having a hard or a soft density profile.
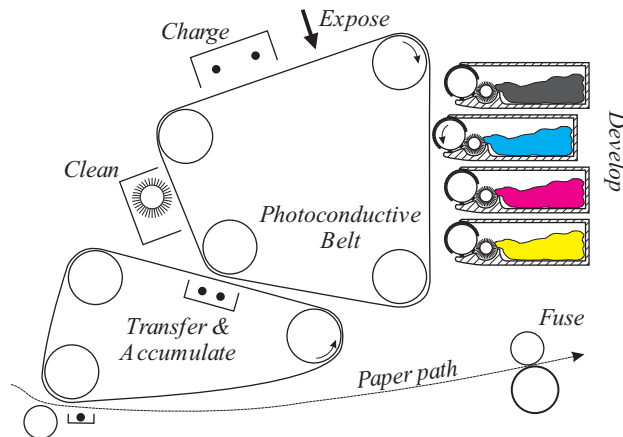
Figure 1. The electrophotographic process.

The presented simulation model simulates the toner layer thickness profile of printed patches starting from an input page bitmap and passing through all the main electrophotographic printing process steps shown in Fig. 1. These steps comprise the exposure of the printed bitmap, the forming of the attracting electrostatic field, the toner's random charge and diameter distributions, the toner transfer and color accumulation, as well as the fusing step.[1,2]

Applying Bouguer-Lambert's law, the simulated micro thickness profiles are converted to color transmittance spectra which yield a very good prediction of the measured spectra of patches printed on overhead transparencies.

2. MODELING THE ELECTROPHOTOGRAPHIC PROCESS

The proposed simulation model[3] considers a microscopic scale with a resolution of 6.0 μm. In order to simulate the effects of each significant process step, a 2×2 mm wide color patch is simulated and passed from one sub-model to the others. In this paper, we demonstrate the simulated effects using an illustrated evolution of a 210×210 μm magnified input bitmap section of a randomly covered monochrome patch with an intended surface coverage of 32% (Fig. 2 upper left side).

The surface of the photoconductive plate is assumed to be homogeneously charged during the charging step. Its surface charge is considered to be neither dependent on the current bitmap nor on the previously printed ones. In order to predict the deposited toner layers, the first significant process step is the constitution of the attracting electrostatic field formed by the "bitmap exposed" photoconductive plate.

2.1. Electrostatic Field of an Exposed Bitmap

For pictorial electrophotography, the most suitable computation scheme for modeling the attracting electrostatic field of a "bitmap exposed" photoconductive plate, relies on a circular convolution kernel. This kernel, whose approximation is described below, must characterize the attracting field of a *single* exposed dot in the vicinity of a development electrode.

Neugebauer and others have shown that the density of an electrophotographic image, is essentially given by the perpendicular component of the electrostatic field above the photoconductive plate. In his publications,[4,5] Neugebauer has introduced $C(k)$, a Modulation Transfer Function (MTF) relating the electrostatic field to the line exposure of a photoconductor:

$$C(k) = \frac{A(k)}{B(k)} \cosh(k(L_1 - z)), \tag{1}$$

where:

$A(k) = \sinh(kL_2) - \frac{\beta}{kL_2}(\cosh(kL_2) - e^{-\beta})$,

$B(k) = (\cosh(kL_1)\sinh(kL_2) + \eta\sinh(kL_1)\cosh(kL_2))(1 - (\frac{\beta}{kL_2})^2)$,

k : exposed line frequency; line pairs per 2π microns,
L_1 : distance between the development electrode and the photoconductive plate,
L_2 : thickness of the photoconductive plate,
β : function of L_2, drift mobility, trapping time and the initial plate voltage,
η : dielectric constant of the plate,
z : average distance between the electrophotographic plate and the charges of the toner particles which will be developed.

In the case of line exposure, the perpendicular electrostatic field component $E_z(x)$ of a particular printer can be computed by applying to the intensity profile $I(x)$ of the exposure spot a convolution with the inverse Fourier Transform $c(x)$ of the MTF $C(k)$:[1]

$$E_z(x) = I(x) * c(x), \tag{2}$$

where:

x : spatial coordinate,

c : Fourier-Transform of $C(k)$, evaluated numerically

I : saturated gaussian intensity profile given as follows: $I(x) = \begin{cases} \tau_{exp} & : x \in [x_1, x_2] \\ I_0 e^{-0.5(x/\alpha)^2} & : \text{otherwise} \end{cases}$,

τ_{exp} : saturation,
x_1, x_2 : solution x of $I(x) = \tau_{exp}$,
I_0, α : constants dependent on the exposure unit.

The circular convolution kernel, $E_z(u, v)$ can finally be approximated by rotating $E_z(x)$ around the vertical axis, which is basically done by substituting x with $\sqrt{u^2 + v^2}$. An example of the resulting dot field approximation is shown in the upper right part of Fig. 2.
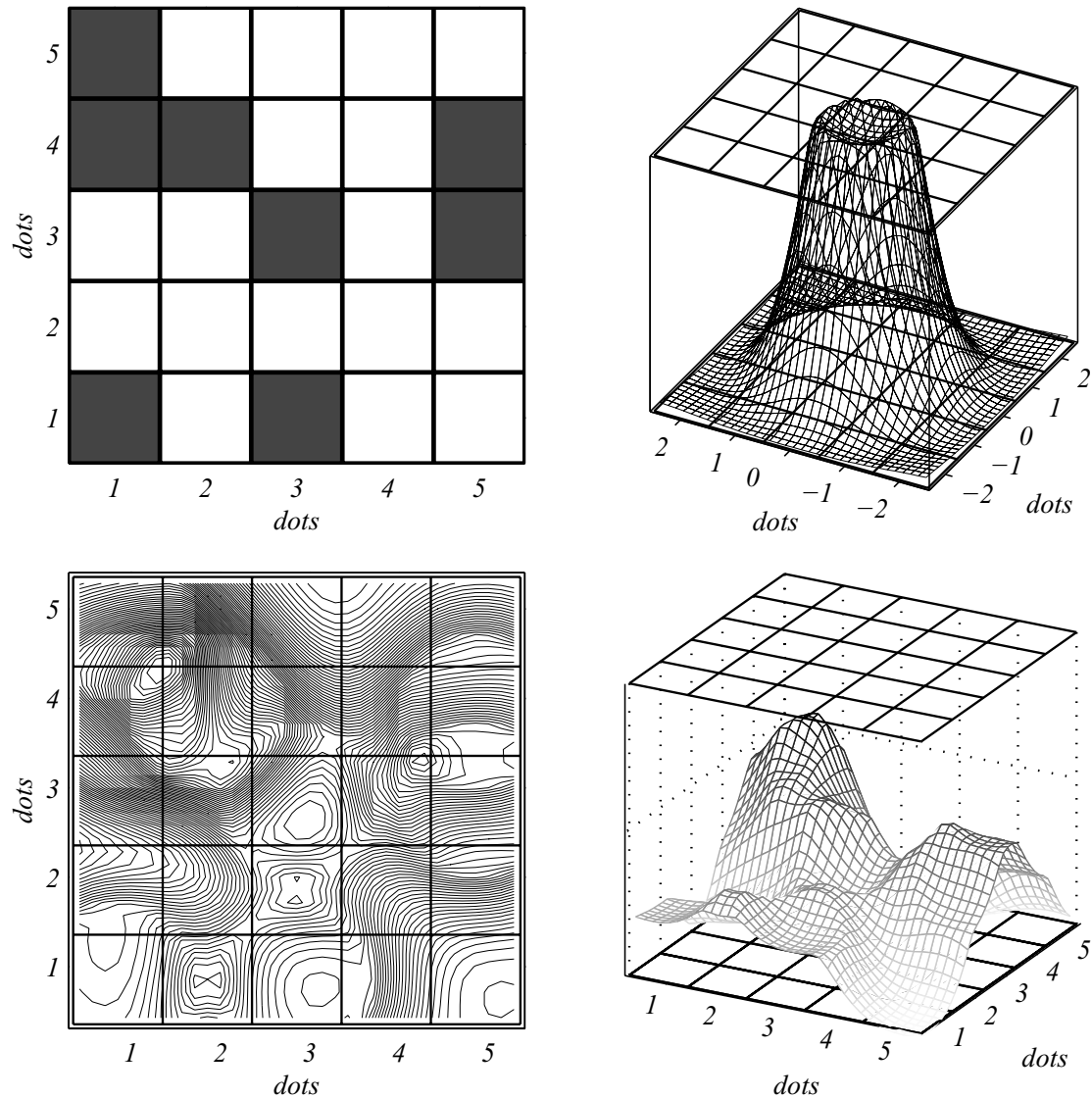
Figure 2. *Upper left*: Enlarged section of an input bitmap. *Upper right*: The perpendicular electrostatic field component of a single dot $(E_z(u, v))$. *Lower left*: Contour plot of the resulting electrostatic field of one color separation (latent image). *Lower right*: Three dimensional representation of the same electrostatic field.

The proposed electrostatic dot field component takes into account most of the significant electrostatic setup parameters involved in the exposure and developer units. These parameters comprise: the shape of the exposure spot, the thickness of the photoconductive plate, the distance of the plate to the development electrode, an average charge height above the plate of the toner particles which will be developed, the initial plate voltage as well as its dielectric constant. For any exposed bitmap, the overall perpendicular component of the attracting electrostatic field which forms the latent image, can now be easily obtained by superposing the electrostatic field component of a single dot at each exposed dot location (Fig. 2, lower part).

2.2. Image Development

In the developer nip, the obtained latent image is transformed to a visible image by depositing toner particles on the photoconductor according to the attracting electrostatic field. For simplicity, we assume that the deposition of the particles occurs as soon as the attracting perpendicular component of the Coulomb force is strong enough to overcome the impeding adhesion force threshold:

$$qE_z > \tau_{imp} \,, \tag{3}$$

where:

E_z : perpendicular component of the electrostatic field,
q : charge equivalent of a toner particle,
τ_{imp} : adhesion force threshold.

2.3. Toner Charge and Size Distributions

It is known that the toner particles size and charge are distributed in a statistical manner due to the toner grinding and charging processes. Moreover, as the developer unit ages, the toner characteristics can significantly vary.

According to equation (3), the charge distribution influences the development behavior, whereas the size distribution mainly affects the micro transmittance structure of the printed result (as will be shown in *Sec. 3*). In order to model the toner charge and size distributions, let us introduce a lognormal based probability density (pdf) function describing the toner charge (q) characteristics:
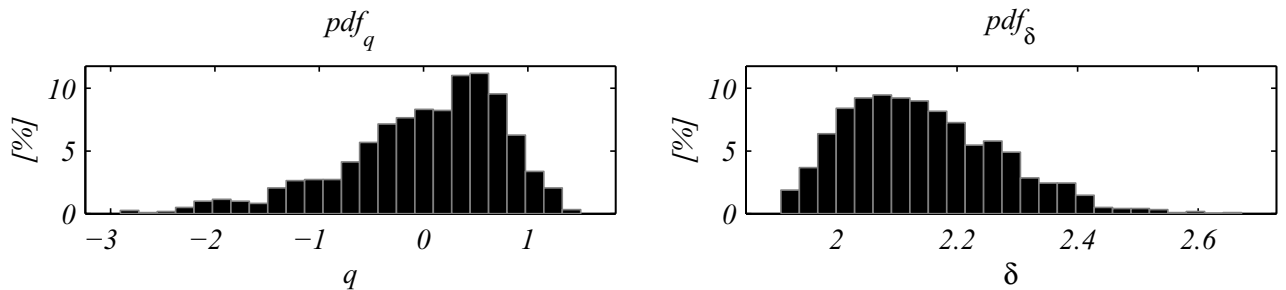
$$pdf_q(\kappa) = \gamma - \frac{1}{\kappa\,\sigma\sqrt{2\pi}}\, e^{\frac{-(\ln \kappa - \mu)^2}{\sigma^2}} \,, \tag{4}$$

and a Rayleigh based function describing the particles diameter (δ) distribution:

$$pdf_\delta(\kappa) = a + \frac{\kappa}{b^2}\, e^{\frac{-\kappa^2}{2b^2}} \,, \tag{5}$$

where:

γ, σ, μ : constants dependent on the toner's charge characteristics,
a, b : constants dependent on the toner's diameter characteristics.

Figure 3. An example of the simulated toner particles charge and size distributions.

The distributions shown in Fig. 3 were selected to match the general shapes reported in various measurements found in the literature.[6] The development condition (eq. 3) is evaluated at each pixel of the high-resolution simulation frame (7×7 *pixels per bitmap dot*) with a random charge according to pdf_q. Where the condition is fulfilled, the initially zero valued pixel is replaced by a particle having a random diameter according to pdf_δ.

2.4. Image Transfer for Two Toner Layers

During the transfer process step, the developed toner particles of each color layer are transported from the photoconductor to a transfer belt. Dependent on the technical setup of the printer, this belt accumulates the different color layers stacked on top of each other. Finally, they are transported simultaneously to the printing medium. During this whole process, the toner particles can either be rejected, repulsed or displaced, and generally, an interference between the color layers cannot be avoided. We assume, that the main effect of this step can be characterized by a transfer efficiency factor ε describing the rejected and repulsed part of the particles.

We subdivide the transfer efficiency of each toner layer into two components. An independent *Auto Transfer Efficiency*, ε_c, describing the lack of transfer of a single layer in the absence of the other color layers. Having N simulated high-resolution pixels, the affected transfer part is modeled by randomly selecting $N(1-\varepsilon_c)$ pixels from the developed image and reducing their toner diameters in a stochastic manner. For a color c, the transferred image can be formulated as:

$$Tr_c = Dv_c - \Delta(\varepsilon_c),\tag{6}$$

where:

Tr_c : simulation frame with the diameter of the transferred toner particles,
Dv_c : simulation frame with the diameter of the originally developed particles,

$\Delta(\varepsilon_c)$: frame of random diameter reduction values: $\Delta(\varepsilon_c)_{(i,j)} = \begin{cases} \varrho : (i,j) \in \Theta(\varepsilon_c)\,,\, \varrho \in]0,1] \\ 0 : \text{otherwise} \end{cases}$,

ϱ : uniform distributed random diameter reduction value at the location (i,j) of the simulation frame,
$\Theta(\varepsilon_c)$: randomly selected set of $N(1-\varepsilon_c)$ affected locations of the simulation frame.

For the second component we introduce a *Cross Transfer Efficiency*, ε_{c_1,c_2} describing the influence of an additional printed color layer c_2 on the layer c_1. The influence of layer c_2 on layer c_1 is modeled by randomly reducing the toner diameters of the color layer c_1 due to the interactions with the layer c_2. We assume that these interactions takes only place at $N_\chi(1-\varepsilon_{c_1,c_2})$ of the pixels which contain, within a 3×3 neighborhood, at least one developed toner particle in each of the superposed layers. N_χ is the total number of pixels fulfilling this condition. Taking into account the neighborhood allows to consider the electrostatic interactions between neighboring particles located in two different layers.

gray value: resulting diameter size
(black: maximum; white: zero)
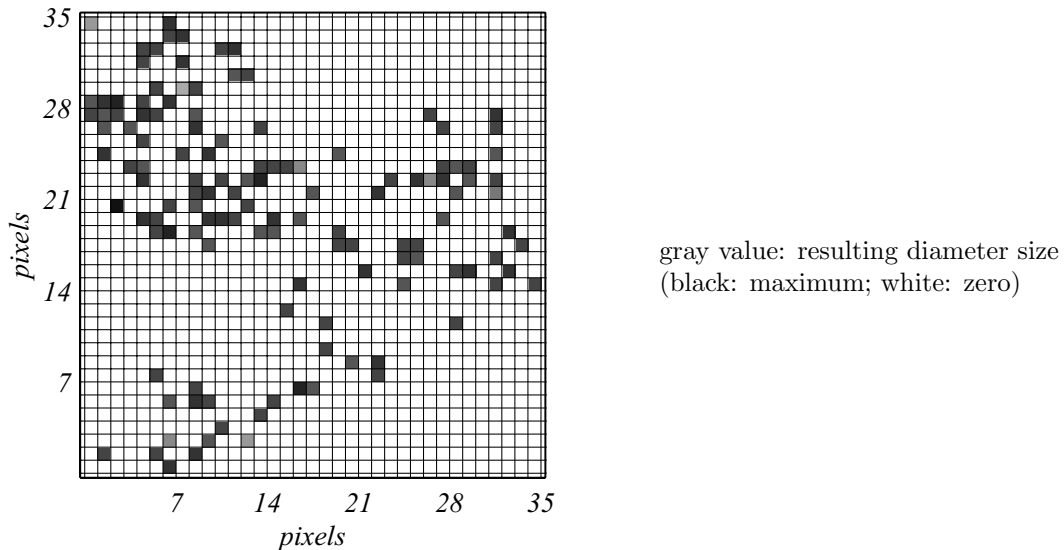
Figure 4. Simulation of transferred single layer toner particles.

For two color superpositions we consider ε_{c_1}, ε_{c_2}, ε_{c_1,c_2} and ε_{c_2,c_1} which have to be optimized with a learning set of printed patches (see Sec. 4). After the complete multi-layer transfer step we obtain for each color layer an image containing the final transferred toner particles having randomly distributed diameters (Fig. 4).

2.5. Fusing Step

After transferring the toner layers to the printing medium, the image is fixed permanently by melting the toner to the medium. The main effects of the fixing heat and pressure within the fuser nip, such as toner flow, spread and particles join are simulated by applying on the transferred particles a smoothing filter. The filter's convolution kernel is based on a hyper-parabola:

$$H(\rho) = \begin{cases} 1 - (\frac{\rho}{\sigma_f})^4 : \rho \in [-\sigma_f, \sigma_f] \\ 0 \qquad : \text{otherwise} \end{cases}, \tag{7}$$

with:

σ_f : average fuser spreading width.

This filter operation yields the micro thickness profile $\delta_{c,i}$ (Fig. 5) for each color layer c and each simulation pixel i. It is the key element for the subsequent transmittance spectrum calculation.
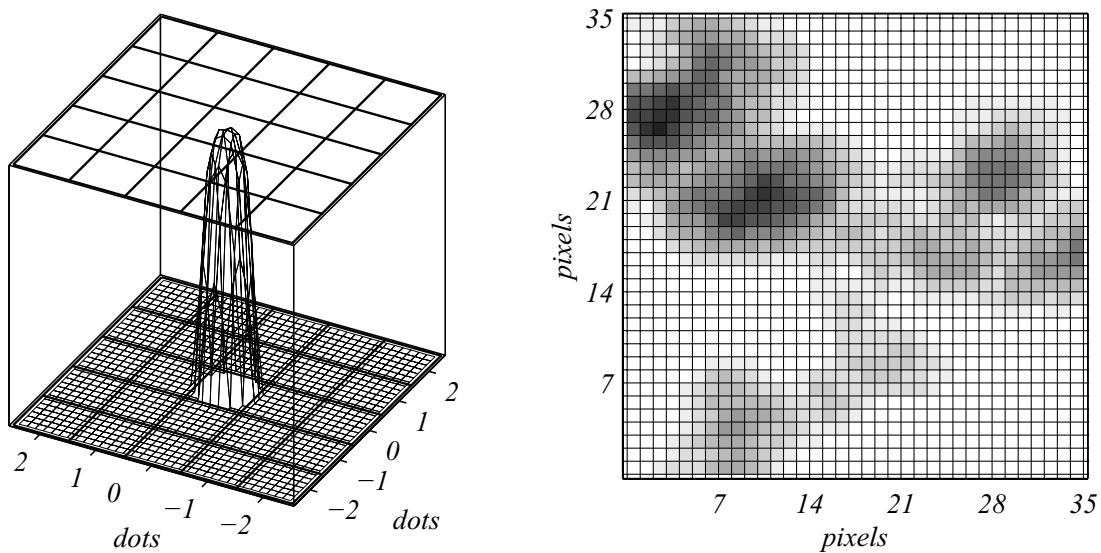
Figure 5. *Left*: Convolution kernel used to simulate the effect of the fuser on the transferred toner particles. *Right*: Fusing simulation of the transferred monochrome toner layer shown in Fig. 4.

3. COMPUTATION OF THE TRANSMITTANCE SPECTRA

The simulated microscopic thickness profile $\delta_{c,i}$ of each color layer can be transformed pixel by pixel to a transmittance spectrum by applying *Bouguer-Lambert's* law (also called Beer's law).[7] In general, this law can only be applied for non-scattering filters and hence, its applicability for toner layers must be first verified. Extensive colorimetric measurements performed in our lab have confirmed its applicability and shown that predictions based on Bouguer-Lambert's law lead to a maximal mean estimation error of CIE-LAB $\Delta E = 1.5$.

According to Bouguer-Lambert's law, we can express the spectral transmittance of a filter of relative thickness δ as:

$$\vartheta(\lambda) = \left[\vartheta_{ref}(\lambda)\right]^{\delta}, \tag{8}$$

where:

λ : wavelength of light,
ϑ_{ref} : spectral optical transmittance of a filter with a reference thickness,
ϑ : unknown spectral transmittance of a filter with the same extinction coefficient and a new layer thickness,
δ : relative thickness of the unknown filter.

$\vartheta_{ref}(\lambda)$ is substituted by the macroscopic measured color transmittance of a solid patch $T_{100\%}(\lambda)$. The relative thickness δ is given by the simulated relative thickness profile $\delta_{c,i}$ derived in Sec. 2.5. In order to compute the macroscopic color transmittance $T(\lambda)$ of a multi-color print, the product of the microscopic spectral contributions of each layer has to be taken and collected over all pixels of the high-resolution simulation frame as follows:

$$T(\lambda) = \frac{1}{N} \sum_{i=1}^{N} \prod_{c=1}^{M} \left[T_{c_{100\%}}(\lambda) \right]^{\delta_{c,i}},$$ (9)

where:

$T_{c_{100\%}}$: measured macroscopic spectral transmittance of a solid patch of the primary color c,
T : macroscopic spectral transmittance of a simulated patch,
$\delta_{c,i}$: simulated thickness at the pixel i of the color layer c,
M : number of over-printed primary colors,
N : total number of simulated pixels.

The obtained transmittance $T(\lambda)$ is a very good prediction of the spectrum that would be obtained using a macroscopic measuring spectrophotometer.

4. EXPERIMENTAL RESULTS

To fit the numerous model parameters, 5 cyan and 5 magenta monochrome patches as well as 4 dual-color (blue) patches were printed on a transparency using a *Tektronix Phaser560 E*. This learning set patches were measured with a *X-Rite DTP41UV/T* spectrophotometer and presented as an optimization goal to a constrained non-linear optimization routine, implemented in MATLAB.[8] After a completed optimization run, the parameters were fixed and tested using a verification set consisting of 400 blue patches with different area coverages. The verification set was printed on a different transparency, one week after the learning set.

Color	ΔE_{mean}	ΔE_{max}
Prediction error	2.5	± 5.5
Process Color Deviations	1.6	± 5.0
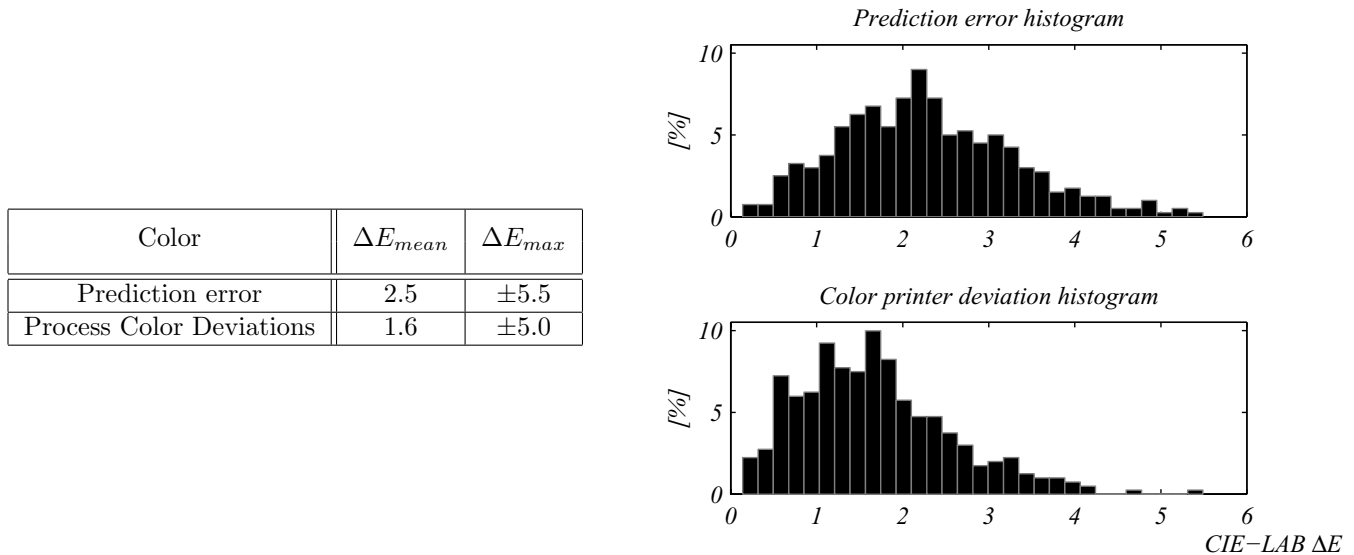
Figure 6. Prediction error and the color deviation when printing on two transparencies for comparison purposes.

The table shown in the left part of Fig. 6 summarizes the obtained prediction error for the blue wedge. The prediction error is compared with the process color deviations. The process color deviations have been measured with a verification set of blue patches printed on different transparencies on the same day.

5. CONCLUSIONS

This paper introduces a simplified simulation model of the electrophotographic process focused on the colorimetric significance of the involved printing process steps. It is based on a MTF for defining the electrostatic field above the photoconductor and on toner particles of random charge and random diameter simulating the impact of the developing electrostatic forces acting in the developer nip of the printer. A simulation of the relative thickness profile of the fused toner particles is obtained by modeling the transfer and the fusing steps. The relative toner thickness profile of each toner layer yields the simulated color transmittance spectra permitting the optimization and evaluation of the model's performance.

The major focus of the simulation model is the prediction of color transmittance spectra of homogeneous electrophotographic printed patches. The prediction carried out for two color toner layers is of a high accuracy (CIE-LAB $\Delta E_{mean} = 2.5$). This prediction cannot be much improved since the printer's printing deviations (process noise) have a similar value. This research is currently being extended to 3 toner layers and to paper support.

REFERENCES

1. E. M. Williams, *The Physics and Technology of Xerographic Processes*, John Wiley & Sons, Inc., 1984.
2. L. B. Schein, *Electrophotography and Development Physics*, Laplacian Press, rev. 2. ed., 1996.
3. S. Mourad, P. Emmel, and R. D. Hersch, "Predicting monochrome color transmittance spectra of electrophotographic prints," in *NIP16*, pp. 862–866, IS&T, (Vancouver, B.C.), 2000.
4. H. E. J. Neugebauer, "A describing function for the modulation transfer of xerography," *Applied Optics* **4**(4), pp. 453–459, 1965.
5. H. E. J. Neugebauer, "Development method and modulation transfer function of xerography," *Applied Optics* **6**(5), pp. 943–945, 1967.
6. R. J. Nash, M. L. Grande, and R. N. Muller, "The effect of toner and carrier composition on the average and distributed toner charge values," in *NIP14*, pp. 332–340, IS&T, (Toronto, Ontario), 1998.
7. G. Wyszecki, *Color Science*, John Wiley & Sons, Inc., 2. ed., 1982.
8. *Optimization Toolbox*, MathWorks, 1999.